J. Synchrotron Rad. (2000). **7**, 131–138

Feasibility and review of anomalous X-ray diffraction at long wavelengths in materials research and protein crystallography

Richard Kahn,[a] Philippe Carpentier,[a] Carmen Berthet-Colominas,[b] Maria Capitan,[c] Marie-Laure Chesne,[a] Eric Fanchon,[a] Stéphane Lequien,[c,e] Dominique Thiaudière,[c] Jean Vicat,[a] Piotr Zielinski[f] and Heinrich Stuhrmann[a,d]*

[a]Institut de Biologie Structurale Jean Pierre Ebel, CEA/CNRS, Grenoble, France, [b]European Molecular Biology Laboratory, Outstation Grenoble, France, [c]European Synchrotron Radiation Facility (ESRF), Grenoble, France, [d]GKSS Forschungszentrum, Geesthacht, Germany, [e]CEA, Saclay, France, and [f]Institute of Nuclear Physics, Kraków, Poland. E-mail: heinrich.stuhrmann@ibs.fr

(*Received 8 September 1999; accepted 5 January 2000*)

The feasibility and a review of progress in the long-wavelengths anomalous dispersion technique is given in the context of the development of beamline ID1 of the ESRF for such studies. First experiments on this beamline and their analyses are described. The first study reports on the use of uranium which exhibits an unusually strong anomalous dispersion at its M_V absorption edge (λ_{M_V} = 3.5 Å). The anomalous scattering amplitude of uranium with 110 anomalous electrons exceeds the resonance scattering of other strong anomalous scatterers like that of the rare earth ions by a factor of four. The resulting exceptional phasing power of uranium is most attractive in protein crystallography using the MAD method. The anomalous dispersion of a uranium derivative of asparaginyl-tRNA synthetase (hexagonal, a = 124.4 Å, c = 123.4 Å) has been measured at three wavelengths near the M_V edge using beamline ID1 of the ESRF. The present set-up allowed the measurement of 10% of the possible reflections at a resolution of 8 Å. This is mainly due to the low sensitivity of the CCD camera. The second study, involving DAFS experiments at wavelengths near the K-absorption edge of chlorine (λ_K = 4.4 Å), reports the use of salt crystals which give rise to much stronger intensities of diffraction peaks than those of protein crystals. In the case of a crystal of pentamethylammonium undecachlorodibismuthate (PMACB, orthorhombic, a = 13.00 Å, b = 14.038 Å, c = 15.45 Å), all reflections within the resolution range from 6.4 Å to 3.5 Å and the total scan width of 24° were collected. The crystalline structure of PMACB implies two chemically distinct states of the Cl atom. Consequently, different dispersions near the K-edge of chlorine are expected. The dispersion of the intensity of five Bragg peaks of the PMACB crystal has been measured at 30 wavelengths. The relative success of these preliminary experiments with X-rays of long wavelength shows that the measurement of anomalous X-ray diffraction at wavelengths beyond 3 Å is feasible. Starting from the experience gained in these experiments, an increased efficiency of the instrument ID1 by two to three orders of magnitude will be achieved in this wavelength range. A comparison with different techniques of anomalous diffraction which rely on the use of argon/ethane-filled multiwire chambers and image plates as detectors for wavelengths near the K-edge of sulfur and phosphorus is also given.

Keywords: long wavelengths; M_V-absorption edge of uranium; K-absorption edge of chlorine; MAD; DAFS.

1. Introduction

The use of soft X-rays in diffraction studies began to develop during the 1990s. The main reason for using soft X-rays in diffraction studies has been in the use of anomalous dispersion. As shown in Table 1, progress was achieved in applications to solid-state physics and protein crystallography almost simultaneously. All exploratory studies of near-edge anomalous diffraction from sulfur and phosphorus in protein crystallography have been performed at HASYLAB (DESY, Hamburg). The other anomalous diffraction projects have been carried out at NLS, Brookhaven National Laboratory. We will now outline the motivation for the use of this technique in structural biology and material science and discuss the technical requirements thereafter.

Table 1
Experiments using anomalous soft X-ray diffraction.

	Edge	E (eV)	λ (Å)	Diffracting sample	Reference
Ni	L_{III}	853	14.53	Reflection from multilayer	Sève, Tonnerre & Raoux (1998)
Si	K	1840	6.74	SAS from SiO_2 particles	Scholl *et al.* (1995)
P	K	2143	5.78	Crystal of ribosome	Stuhrmann, Hütsch *et al.* (1995)
				Filamentous bacteriophage	Welsh *et al.* (1995)
S	K	2470	5.02	Crystal of lysozyme	Lehmann *et al.* (1993)
				Poly(3-octylthiophen)	Mardalen *et al.* (1994)
				Crystal of trypsin	Stuhrmann *et al.* (1996, 1997)
				Crystal of ribosomal protein L8	Thomas (1997)
				Crystal of riboflavin binding protein	Trame (1997)
				Bacteriorhodopsin	Behrens *et al.* (1998)
				Liquid crystal	Mach *et al.* (1998, 1999)
Cl	K	2820	4.40	Ferroelectric crystal	This work
U	M_V	3545	3.50	Crystal of a tRNA synthetase	This work

2. Protein crystallography with soft X-rays

There are essentially two reasons for extending the method of MAD (multiwavelength anomalous dispersion) to the soft X-ray region, *i.e.* to wavelengths greater than 3 Å: (i) strong anomalous dispersion of heavy elements at the M_{IV}/M_V absorption edges; (ii) access to anomalous dispersion of light elements (Cl, S, P) at their K-edges.

2.1. *Use of the M_{IV}/M_V absorption edges of heavy elements*

Heavy atom labels are introduced into the native protein by co-crystallization, by diffusion into the protein crystal (soaking), or by binding the label atom to the protein before crystallization (*e.g.* Se). Ideally the heavy atom will be bound to the surface of the protein, leaving the protein structure undisturbed. The heavy metal derivative of the protein crystal is then isomorphous to the native crystal. In practice, there may be numerous reasons for imperfect isomorphism, which may become apparent at higher structural resolution. The MAD method does not suffer from such a shortcoming because an effect analogous to isomorphous replacement is generated with just one protein crystal by varying the wavelength through the absorption edge.

Among the heavy atoms, uranium is the most powerful scatterer. This is true both for the off-resonance scattering because of its atomic number $Z = 92$ and for the contribution from anomalous scattering which exceeds 100 anomalous electron units (Hendrickson & Ogata, 1997). The best anomalous scatterers at wavelengths below 3 Å are the lanthanides at their L_{III}-absorption edges with up to 30 anomalous electrons. The often-used selenium, mainly as selenomethionine in proteins, offers eight anomalous electrons at its K-absorption edge (Fig. 1). Using the MAD method, uranium derivatives exhibit both the highest phasing power and perfect isomorphism. This is crucial for the determination of large structures ($M > 500$ kDa).

2.2. *Use of the K-absorption edges of light elements*

Light elements, such as calcium, chlorine, sulfur and phosphorus, are tremendously important in living organisms. Phosphorus is an integral part of RNA/DNA and of nucleotides, like ATP. Sulfur is an integral part of proteins and therefore an essential element for life.

In many cases sulfur in proteins is substituted almost routinely by selenium by replacing methionine by selenomethionine. Then the use of the anomalous dispersion of selenium at the K-absorption edge at 0.978 Å is definitely to be preferred. However, there are a non-negligible number of proteins where neither substitution by selenium nor isomorphous substitution can be used. This is the case for apocrustacyanine C1 ($M = 20$ kDa), a protein with three putative disulfide bridges (40 kDa and six disulfide bridges

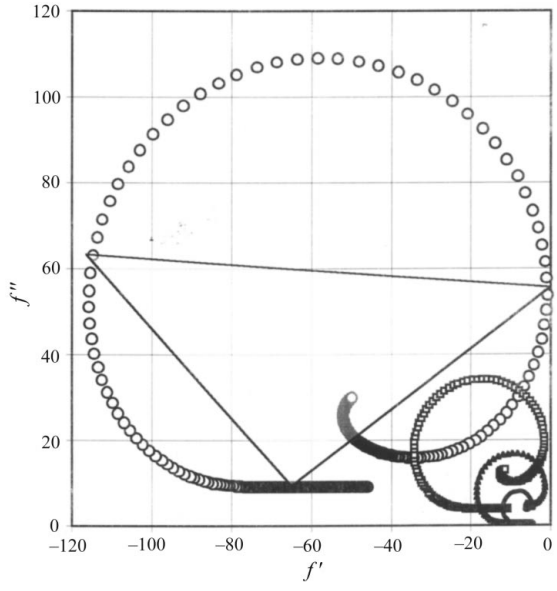

Figure 1
The anomalous dispersion of some elements (in electron units). Circles: M_V-edge of uranium in uranyl acetate; squares: L_{III}-edge of lanthanide ions; triangles: K-edge of phosphorus (DNA); line: K-edge of selenium in selenomethionine. The imaginary part f'' is plotted *versus* the real part f' of the atomic form factor. The points denote $f' + if''$ in the plane of complex numbers at an energy spacing of 0.1 eV. The curves are almost closed circles. Measurement of the diffracted intensity for one Bragg peak at three wavelengths is sufficient for its phase determination.

for one dimer in the crystallographic asymmetric unit), lacking methionine and not forming an isomorphous derivative with a heavy metal (Cianci *et al.*, 1999). The structure of a similar but smaller protein of that type, crambin (M = 6 kDa), has been solved by Hendrickson & Teeter (1981) using the differences of intensities of Bijvoet pairs for phasing Bragg reflections. The diffraction experiment was performed at a wavelength of 1.54 Å where the imaginary part of the resonant scattering amplitude of sulfur, f'', giving rise to unequal intensities of Bijvoet pairs amounts to 0.5 electron units (short bar in Fig. 2). Hence the three disulfide bridges of crambin yield to a mean variation of 1.4% in the diffraction ratio $\langle|F_{\mathbf{h}} - F_{-\mathbf{h}}|\rangle/\langle F\rangle$ (Hendrickson & Teeter, 1981).

As $|F_{\mathbf{h}} - F_{-\mathbf{h}}|$ is proportional to f'', larger intensity differences between Bijvoet pairs are expected at larger wavelengths λ. The increase of f'' as λ^2 is a reason to use wavelengths between 2 Å and 2.5 Å where conventional diffraction techniques are expected to give satisfactory results. No results from such measurements have been reported yet. The longest-wavelength anomalous dispersion structural result is that obtained using the Daresbury SRS at the Mn K-edge (1.896 Å) to successfully distinguish Mn from Ca in pea lectin (Einspahr *et al.*, 1985).

Recently the question whether the anomalous signal of sulfur can become a tool for solving protein structures has been addressed by Dauter *et al.* (1999). It appears that this goal can be achieved for well diffracting crystals (at least 1.2 Å resolution) thanks to modern more accurate data-collection techniques and new statistical phasing algorithms. Using a synchrotron radiation wavelength of 1.54 Å, ten S and seven Cl atom positions were determined from their anomalous signal and an electron density map of high quality was obtained (Dauter *et al.*, 1999).

Note that the mathematical methods for phasing Bragg reflections in the presence of numerous resonant scatterers per protein molecule has seen considerable progress with the advent of selenium derivatives. These methods are likely to facilitate the use of anomalous dispersion from sulfur in native proteins.

Phosphorus in RNA/DNA is a unique resonant label as it cannot be replaced by its heavier homologue, arsenic. As each nucleotide contains one P atom, the concentration of phosphorus in RNA/DNA may reach several moles l^{-1}. The concept of contrast becomes applicable. The analysis of the anomalous diffraction at wavelengths near the K-edge of phosphorus then will be performed in a way which is being developed for MASC (multiwavelength anomalous solvent contrast) (Fourme *et al.*, 1995). This method is suitable for the low-resolution maps of P atoms in large particles, like viruses, ribosomes (Stuhrmann, Hütsch *et al.*, 1995) and phages (Welsh *et al.*, 1995).

Apart from the use of MAD for solving the phase problem, soft X-rays can be used for DAFS (diffraction anomalous fine-structure) experiments to obtain information on the chemical state of atoms at specific sites in the unit cell. This method is becoming very important for the study of small molecules, as will be shown below.

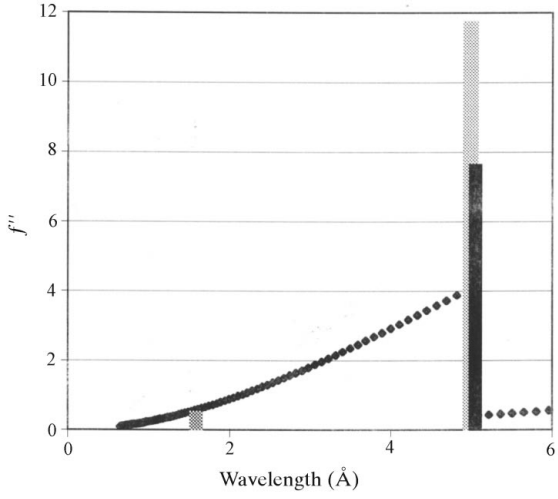

Figure 2
Anomalous dispersion of f'' of sulfur. To a good approximation, f'' increases with the square of the wavelength until it reaches a maximum of 4.1 electron units (eu) at the K-absorption edge of sulfur at 5.02 Å. There is an overshoot of f'' and a shift of the edge which depends on the chemical state of sulfur. The edge of sulfur in sulfides is at 5.018 Å or 2470 eV (black bar) and that of sulfates is at 5.00 Å or 2480 eV (grey bar). At the edge the dispersion of sulfate with $f_{max}'' \simeq 12$ eu is stronger than that of sulfur in methionine or cystein with f_{max}'' close to 7 eu. The crystal structure of crambin has been solved by using a wavelength of 1.5 Å, indicated by a short bar (Hendrickson & Teeter, 1981), whereas in more recent studies the MAD method was used at wavelengths close to the K-absorption edge of sulfur (Stuhrmann *et al.*, 1997).

3. Soft X-ray diffraction in soft matter research

There have been numerous EXAFS studies with soft X-rays (for a review, see George, 1993). Most of the ground-breaking applications are found in the Activity Reports of the SSRL (Stanford Synchrotron Radiation Laboratory). Many concern sulfur in its various chemical states. This also holds for the corresponding, and much less numerous, diffraction experiments (Table 1). Diffraction of soft X-rays at wavelengths near the K-edge of sulfur have been performed on polymers (Mardalen *et al.*, 1994) and on liquid crystals (Mach *et al.*, 1998, 1999). In the experiments on liquid crystals, Mach *et al.* (1999) made use of the tensorial properties of resonant scattering from sulfur at wavelengths near the K-absorption edge in order to characterize various chiral smectic-C phases of thiobenzoate liquid-crystal compounds. This unique approach revealed, for the first time, direct structural evidence of distinct periodicities in several chiral smectic-C phases, including two-layer, three-layer and four-layer superlattices. Polarization analysis identified the polarization state of the satellite peaks arising from these superlattices (Mach *et al.*, 1999). These studies may well be regarded as a most promising start of a more extensive use of anomalous soft X-ray diffraction in polymer and liquid-crystal research.

In fact, they are related to another fast-developing method utilizing anomalous dispersion known as DAFS. In a DAFS experiment a few reflections are selected for a detailed measurement of their dispersions. The intensity of each Bragg reflection is measured at many wavelengths, *i.e.* X-ray absorption spectra are collected at different wavevectors. Hence, DAFS can provide EXAFS- or XANES-like information for a specific subset of atoms selected by the diffraction condition (Sorensen *et al.*, 1994).

These are some of the promising features of soft X-ray diffraction in soft matter research, not to mention the impact on polarized X-ray diffraction studies (Schütz *et al.*, 1994) and resonant magnetic X-ray diffraction (Vettier, 1994) in solid-state physics.

4. Experimental aspects

The studies of the uranium derivative of asparaginyl-tRNA synthetase by the MAD method and of pentamethylammonium undecachlorodibismuthate by DAFS have been chosen essentially for two reasons: (i) they represent cases of scientific interest in structural biology and in solid-state physics, respectively; (ii) and most importantly, they were within the range of technical feasibility of instrument ID1 of the ESRF at the time when the experiments were performed (November and December 1998).

X-ray beams at wavelengths beyond 3 Å are most conveniently obtained at synchrotron radiation facilities. The technique of soft X-ray diffraction is still a technical challenge, as the atmospheric attenuation of the incident and diffracted X-rays is a very significant problem. At the M_V-edge of uranium, for example, 1 cm of nitrogen at atmospheric pressure will absorb 9% of the incident beam and, at the phosphorus *K*-edge, 40% of the radiation would be absorbed. Because of these difficulties, experiments are either conducted in an atmosphere of helium gas or *in vacuo*.

Whereas diffraction X-ray experiments *in vacuo* are not a problem in many disciplines, biological samples require an aqueous environment, which is incompatible with a high vacuum. The use of a helium atmosphere is a good choice at wavelengths below 10 Å.

The penetration depth of soft X-rays in organic material decreases with larger X-ray wavelengths in a way which is quite similar to that of air (Fig. 3). Although the sample volume giving rise to diffraction is reduced considerably at longer X-ray wavelengths, the diffracted intensity is much less reduced. This is because the diffracted intensity, after correction for absorption, increases with the square of the wavelength (Fig. 3). Hence, a small sample volume is not so much of a problem for soft X-ray diffraction. The quality of soft X-ray diffraction data is essentially determined by the concept of the X-ray beamline.

An experimental set-up suitable for the measurement of soft X-ray diffraction was used at HASYLAB until the end of 1996 (Stuhrmann, Hütsch *et al.*, 1995). With that instrument soft X-ray diffraction data from protein crystals was measured up to scattering angles of $2\theta = 120^\circ$ (Stuhrmann *et al.*, 1997) using wavelengths close to the absorption edge of sulfur at 5 Å. Radiation damage turned out to be not too severe, as crystals of lysozyme at 277 K and of trypsin at 193 K kept on diffracting soft X-rays for several hours. The diffracted intensity was measured with four multiwire chambers, all of them using a flow of argon–ethane (10:1). The diffraction pattern from trypsin recorded by one of the detectors is shown in Fig. 4. For comparison the diffraction of 5 Å photons from trypsin was recorded by an image plate (Fig. 5). The data are of similar quality (Stuhrmann, Braunwart & Stuhrmann, 1995).

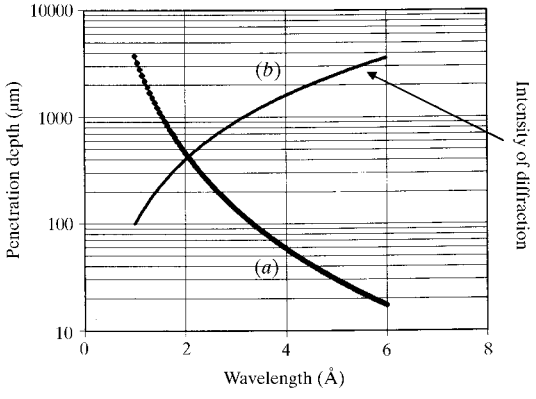

Figure 3
(*a*) Penetration depth of X-rays in water. (*b*) Kinematical scattering intensity (arbitrary units).

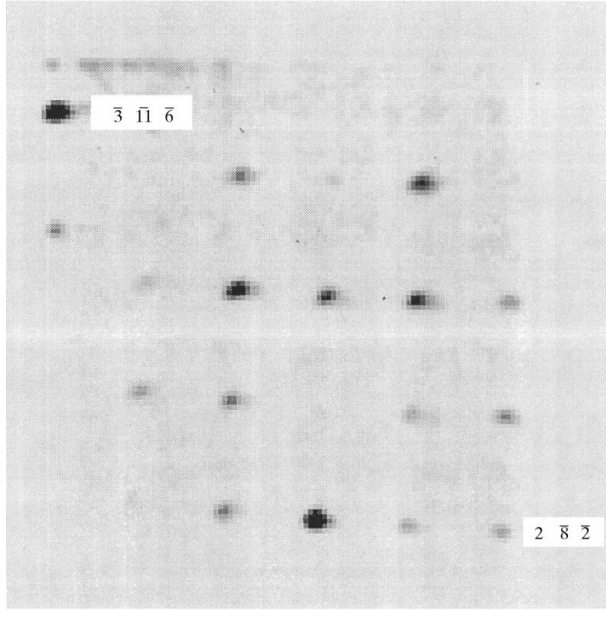

Figure 4
Diffraction of 5 Å photons from a single crystal of trypsin (Stuhrmann *et al.*, 1997). The detector is a 300 × 300 mm multiwire proportional counter (from A. Gabriel, EMBL) filled with argon/ethane at a distance of 55 cm from the protein crystal. The peak height to background ratio for the strongest reflections is 10:1. Oscillation: 1°; time: 2 min at beamline A1 of HASYLAB. This picture is part of Fig. 10.

On instrument ID1 of the ESRF (Fig. 6), anomalous scattering experiments in the photon energy range from $E = 2$ keV ($\lambda = 6$ Å) to $E = 42$ keV ($\lambda = 0.3$ Å) are possible. With its 16 m^3 vacuum vessel, ID1 offers the possibility of performing X-ray diffraction experiments both in a completely evacuated environment and in a helium atmosphere. The Be window separating the ultrahigh vacuum of the storage ring from the instrument, of thickness 200 μm, transmits 20% of the incident 5 Å photons. The transparency of the Be window increases towards shorter wavelengths. These features are beneficial for experiments in the whole wavelength range accessible by ID1. Not all of the planned specifications of ID1 were met at the date when the experiments presented in this paper were performed. The rejection of higher harmonics, a most important prerequisite in soft X-ray diffraction, was not optimal. The detector, a CCD camera, was known to have a low efficiency at wavelengths beyond 3 Å. In spite of these temporary shortcomings, first exploratory experiments were performed at wavelengths between 3.5 Å and 4.5 Å. It was clear from the beginning that these conditions define technical improvements which are also reported in this paper.

Synchrotron radiation from an undulator was monochromated by an Si(111) double-crystal monochromator. The second crystal was slightly detuned to suppress, to some extent, higher harmonics. Its angular offset was controlled by measuring the scattered intensity from a Kapton foil in the beam just behind the monochromator. A more efficient suppression of higher harmonics was achieved by total reflection from a small plane mirror at a distance of 1 m from the sample. No focusing elements were used.

The scattered intensity was detected by a CCD camera (Princeton) with a sensitive area of 50 mm × 50 mm. The efficiency of this detector was estimated to be ∼0.2% for 5 Å photons and ∼2% for 3.5 Å photons. Further technical details vary with each experiment (see below).

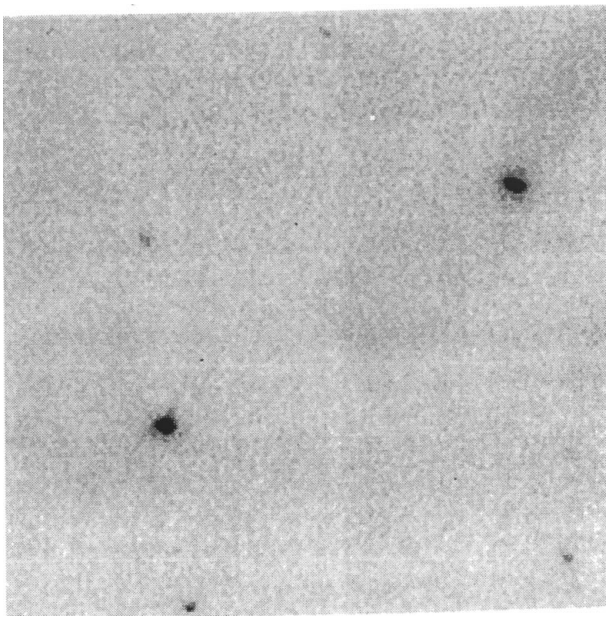

Figure 5
Diffraction pattern of bovine trypsin taken with an image plate (same solid angle as in Fig. 4). Wavelength: 5 Å; oscillation: 1°; exposure time: 10 min. The number of total events per time is similar to that obtained with a multiwire chamber area detector. The crystal is not the same as in Fig. 4 (Stuhrmann, Braunwart & Stuhrmann, 1995).

5. Diffraction experiments at the M_V-edge of uranium

The X-ray absorption spectrum of uranyl acetate has been measured at wavelengths between 3.28 Å and 3.54 Å at the instrument ID1 of the ESRF. The 'white lines' which have been studied by Kalkowski *et al.* (1987) are reproduced well. The dispersion of the imaginary part f'' of uranium at its M_{IV}-edge and M_V-edge was obtained from the absorption spectrum shown in Fig. 7. The spectrum of thorium is quite similar (Kalkowski *et al.*, 1987).

A feasibility test of the MAD method has been performed with the uranium derivative of asparaginyl-tRNA synthetase (two uranium sites per molecule). The same derivative has also been used for the structure determination of this protein (Berthet-Colominas *et al.*, 1998). It crystallizes in the hexagonal space group $P6_422$ with $a = 124.4$ Å, $c = 123.4$ Å. The crystal of the uranium derivative had dimensions of 60 × 60 × 100 μm, which is close to the penetration depth of 3.5 Å radiation (Fig. 3). Hence, the crystal attenuated the incident X-rays by a factor of three.

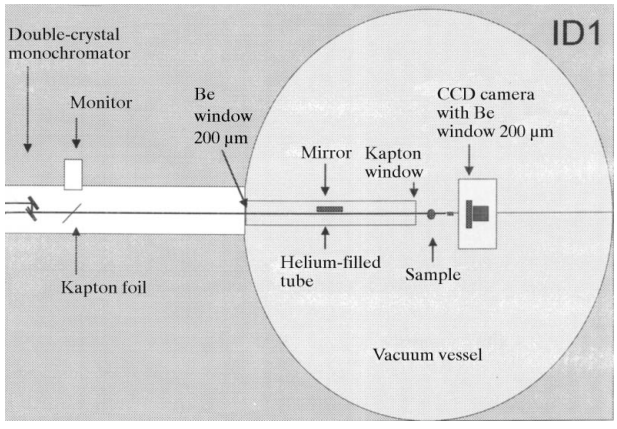

Figure 6
A schematic presentation of the instrument ID1 at the ESRF. Synchrotron radiation from an undulator, monochromated by an Si(111) double-crystal monochromator, enters the hutch through a Be window. For wet samples the soft X-radiation passes through a helium-filled tube of length 1.5 m. No helium path is required for samples which are stable *in vacuo*. The CCD camera can be operated both *in vacuo* and at atmospheric pressure. The diameter of the cylindrical vessel is 2.6 m. The diffractometer (not shown) occupies the bulk of the volume of the vessel.

The temperature of the crystal was kept at 100 K by a flow of cold nitrogen gas. Consequently, the large vessel of ID1 could not be evacuated and a helium path of length 1.5 m between the beryllium window and the sample had to be installed. The air gap of 80 mm between the end of the helium path and the CCD camera reduces the intensity by a factor of three. The beryllium window of thickness 200 μm and the plastic window at the end of the helium path decrease the incident beam by a factor of 2.6.

The sensitive plane of the detector was at a distance $d \geq 48$ mm from the sample. Two kinds of detector orientations were used covering the intervals of scattering angles (0°, 60°) and (–30°, 30°).

Data were recorded up to 8 Å resolution while the orientation was varied in steps of 1° over an interval of 48°, at normal incidence of the primary beam. No diffraction peaks were observed at higher resolution, which would have been accessible with the detector inclined at 30°.

Three wavelengths near the M_V-absorption edge of uranium were used. Below the M_V-absorption edge, at λ = 3.52 Å, 150 peaks were measured while 1500 reflections were expected. The limiting peak intensity was taken at 3σ above the local background. There were still numerous spurious peaks. Hence, only a quarter of the measured peaks were indexed (Fig. 8). The yield of reliable data is even lower at wavelengths close to the absorption peak of the M_V-edge. The main reason for the small number of observed reflections is the low efficiency of the CCD detector. In addition to the noise level of the detector there was a high background scattering mainly from the mirror at a distance of 1 m from the sample (Fig. 6).

6. Diffraction experiments at the *K*-edge of chlorine

The choice of pentamethylammonium undecachlorodibismuthate (PMACB) for our studies has been guided by the following two arguments.

(i) PMACB is a ferroelectric substance below 307 K. The transition from the ferroelectric to the paraelectric state is accompanied by a change of the space group from $Pca2_1$ to $Pcab$. The latter is centrosymmetric (a = 13.003 Å, b = 14.038 Å, c = 15.450 Å). The Cl atom between two Bi atoms of the undecachlorodibismuthate anion, $Bi_2Cl_{11}^{5-}$ (shown in the following scheme) will move from an asymmetric position to a symmetric one. DAFS can, in principle, single out this Cl atom.

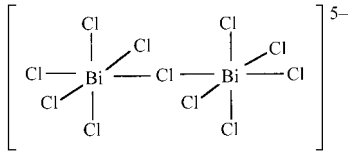

(ii) PMACB is perfectly stable *in vacuo*, even slightly above room temperature. It gives rise to intense X-ray diffraction peaks using laboratory sources. These are promising technical conditions for X-ray diffraction at wavelengths near the K-edge of chlorine at λ_K = 4.4 Å (E_K = 2820 eV), in spite of an efficiency of the CCD camera which is even lower than with the previous example.

The detector plane at a distance of 66 mm from the sample was inclined by 40° with respect to the incident beam covering scattering angles 2θ between 30° and 70°.

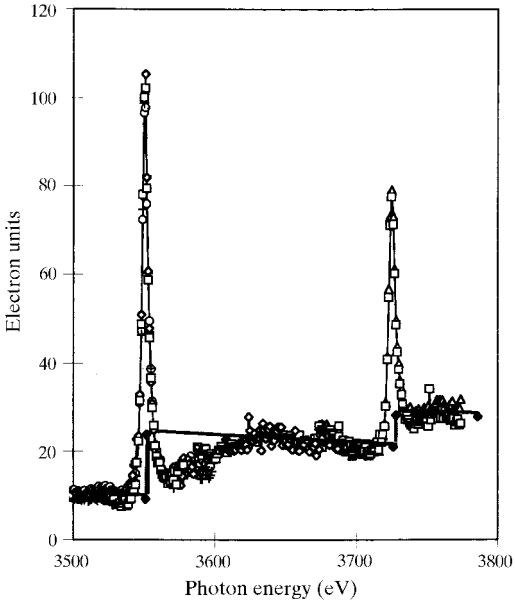

Figure 7
Dispersion of the imaginary part f'' of uranium in uranyl acetate near the M_{IV}-edge and M_V-edge. The absorption spectrum was taken at different undulator gaps and merged thereafter.

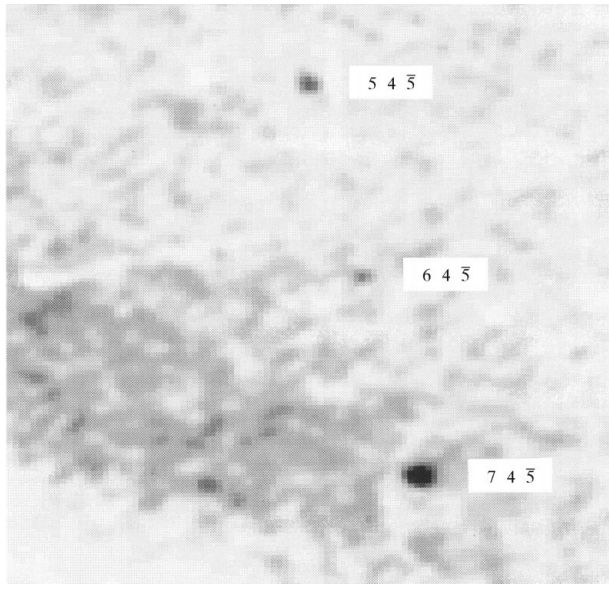

Figure 8
Diffraction of 3.5 Å photons from the uranium derivative of asparaginyl-tRNA synthetase. The weak Bragg peaks are on a high non-uniform background which has been subtracted. The residual background (this figure) is marked by numerous spurious peaks. The peak height to original background ratio of the 7 4 $\bar{5}$ reflection is 1/3. The data were recorded using a CCD camera.

The diffraction experiments were carried out at 323 K, well above the temperature of the phase transition at 307 K. The orientation of the crystal was varied in steps of 2° over an interval of 24°. At each orientation slot the diffracted intensity was measured at 30 energies between 2807 and 2837 eV.

The diffraction pattern turned out to be dominated by reflections due to the third-order harmonic ($\lambda = 1.467$ Å) of the incident radiation (the second-order harmonic is not transmitted by the monochromator). This surprising result is explained by (i) the low efficiency of the CCD camera for 4.4 Å radiation, (ii) the presence of the strongly absorbing 200 μm Kapton foil (needed for the control of the monochromator), which reduces the incident 4.4 Å radiation by a factor of 200, (iii) the very weak but non-negligible reflection of the 1.467 Å radiation by the mirror. The CCD camera is very sensitive to this radiation.

The intensities of the reflections at a given wavelength did not vary to an extent, which might have betrayed the presence of the fundamental wavelength with some of them by an increased intensity.

The answer to this problem was provided by indexation. All reflections due to the fundamental wavelength of 4.4 Å were found and all of them showed a strong variation of the diffracted intensity due to anomalous dispersion and absorption at the *K*-edge of chlorine (Fig. 9). The intensity of the reflections due to the third harmonic radiation was used for calibration. The fluorescence spectrum of chlorine as obtained from the background images, although very weak, was clearly present.

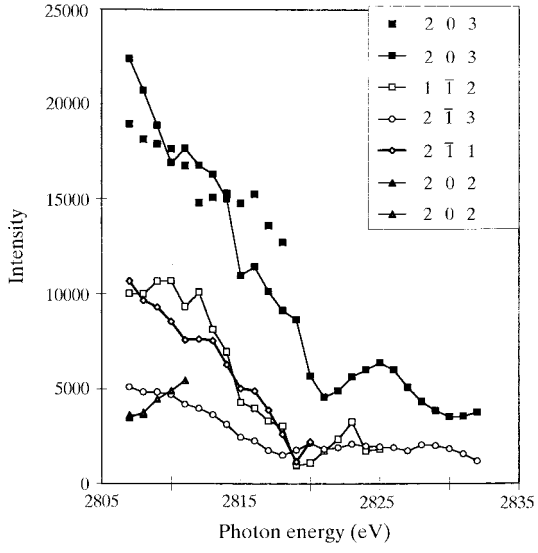

Figure 9
Dispersion of the diffracted intensity of various Bragg reflections near the absorption edge of chlorine. A part of the dispersion of the intensity of the 203 reflection has been measured twice: the slightly different trend of the dispersion of this reflection may be due to a change in the position of either the sample or the monochromatic beam.

There is a slight variation of the dispersion at the *K*-edge of chlorine with the wavevector indicating the sensitivity to the two subsets of Cl atoms differing in their electronic state. The 202 reflection is particularly interesting for our purpose because the Cl atom bridging the Bi atoms in the $[Cl_5Bi–Cl–BiCl_5]^{5-}$ anion, in a strategic position during phase transition, and experiencing a change during phase transition, contributes mainly to the partial structure factor of the 11 Cl atoms. A more complete energy scan is therefore of interest.

7. Conclusions

Materials which are stable *in vacuo* are relatively easily amenable to soft X-ray diffraction. The experiments at wavelengths near the *K*-edge of chlorine have shown that the instrument ID1 of the ESRF offers excellent possibilities for the measurement of DAFS up to wavelengths of 5.0 Å with the replacement of Kapton foil, which is now feasible, but also requires the introduction of a bent mirror in front and behind the monochromator, which is now being performed. The gain in intensity of 4.4 Å radiation will be three orders of magnitude over the operating intensity reported on in this paper. Soft X-ray diffraction from wet biological samples will certainly profit from these changes at ID1. It should also be noted that cooling of a sample by cold nitrogen gas works satisfactorily; one test on a tRNA synthetase crystal demonstrated that no significant radiation damage was observed within a few hours of irradiation by 3.5 Å photons.

A more severe challenge is the low efficiency of the CCD detector, more precisely, the fluorescent screen in front of the fibre optics, which converts X-rays into visible light. The thickness of the fluorescent layer in the 'standard' CCD detector is optimized for wavelengths around 1 Å: soft X-ray photons are absorbed over a thin surface layer on the exposed face, and few visible photons crossing the thick material emerge on the opposite face. A much thinner layer of the fluorescent material for this detector is needed for optimal soft X-ray diffraction data recording.

A further test with an image plate confirmed the sensitivity of image plates for soft X-rays. An image plate has two advantages with respect to a CCD camera.

(i) The readout occurs at the side which has been irradiated by X-rays, *i.e.* there is no need to adjust the thickness of the sensitive material. Image plates are then sensitive to hard and soft X-rays (see also Stuhrmann, Braunwart & Stuhrmann, 1995).

(ii) Image plates are flexible; they can be bent into a cylindrical surface, as shown in Fig. 10, covering two-thirds of the unit sphere, important for reaching reasonable *d*-spacing coverage.

Hence, the aperture of the detector is larger.

The simultaneous measurement of a larger number of reflections with an image plate reduces the measuring time and, most importantly, thereby reduces the radiation damage occurring to the sample with time.

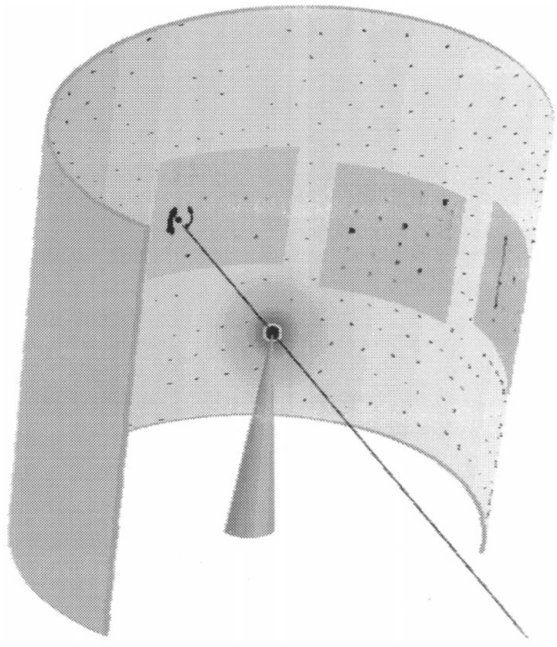

Figure 10
Comparison of the diffraction data from trypsin measured with a set of four multiwire chambers (Stuhrmann, 1997) with the calculated diffraction pattern of the same trypsin crystal projected onto the cylindrical image plate. The scan width is 1°. The incident X-ray beam emanates from the lower right-hand corner, passes the sample on top of the cone and is caught in a beam stop in front of the inner surface of the cylinder. The increased scattering intensity near the beam stop, which has been measured by one of the detectors, is clearly visible. The picture of the neighbouring detector is shown in Fig. 4. The four area detectors (one of them is hidden) accept the following intervals of scattering angles (−50°, −18°), (−5°, 27), (40°, 72°), (85°, 117°). Diffraction peaks from trypsin have been observed in the full range of accessible scattering angles. The four area detectors cover a solid angle of one-tenth of a unit sphere. If a bent image plate had been used, a simultaneous measurement over two-thirds of the unit sphere would have been possible. In the absence of a cylindrical on-line image-plate scanner, a flat on-line image-plate scanner would still be a good compromise.

In conclusion, the ideal experimental set-up sought will include the following: firstly, a sample cooled with cold helium gas and, secondly, the diffraction data recorded by a cylindrical on-line image-plate scanner (Fig. 10). A more conventional on-line image-plate scanner adapted to a helium gas environment would then be a good compromise. Such a configuration would allow for a continuous helium atmosphere from the beryllium window to the detector. The absorption of soft X-rays along the beam path would be very small. Moreover, cold helium would give excellent radiation protection of the protein crystal.

References

Behrens, W., Otto, H., Stuhrmann, H. B. & Heyn, M. P. (1998). *Biophys. J.* **75**, 255–263.

Berthet-Colominas, C., Seignovert, L., Härtlein, M., Grotli, M., Cusack, S. & Leberman, R. (1998). *EMBO J.* **17**, 2947–2960.

Cianci, M., Olczak, A., Mukherjee, A. K., Raftery, J., Rizkallah, P. J., Chayen, N. E., Zagalsky, P. F. & Helliwell, J. R. (1999). Synchrotron Radiation Satellite to the 18th IUCR General Assembly and Congress, Poster Abstract, Daresbury Laboratory, Warrington, Cheshire, UK.

Dauter, Z., Dauter, M., de la Fortelle, E., Bricogne, G. & Sheldrick, G. M. (1999). *J. Mol. Biol.* **289**, 83–92.

Einspahr, H., Sugana, K., Suddath, F. L., Ellis, G., Helliwell, J. R. & Papiz, M. Z. (1985). *Acta Cryst.* B**41**, 336–341.

Fourme, R., Shephard, W., Kahn, R., L'Hermite, G. & Li de la Sierra, I. (1995). *J. Synchrotron Rad.* **2**, 36–48.

George, G. N. (1993). *Curr. Opin. Struct. Biol.* **3**, 780–784.

Hendrickson, W. A. & Ogata, C. M. (1997). *Methods Enzymol.* **276**, 494–523.

Hendrickson, W. A. & Teeter, M. M. (1981). *Nature (London)*, **290**, 107–113.

Kalkowski, G., Kaindl, G., Brewer, W. D. & Krone, W. (1987). *Phys. Rev. B*, **35**, 2667–2677.

Lehmann, M. S., Müller, H. H. & Stuhrmann, H. B. (1993). *Acta Cryst.* D**49**, 308–310.

Mach, P., Pindak, R., Levelut, A.-M., Barois, P., Nguyen, H. T., Baltes, H., Hird, M., Toyne, K., Seed, A., Goodby, J. W., Huang, C. C. & Furenlid, L. (1999). *Phys. Rev. E.* **60**, 6793–6802.

Mach, P., Pindak, R., Levelut, A.-M., Barois, P., Nguyen, H. T., Huang, C. C. & Furenlid, L. (1998). *Phys. Rev. Lett.* **81**, 1015–1018.

Mardalen, J., Riekel, C. & Müller, H. (1994). *J. Appl. Cryst.* **27**, 192–195.

Scholl, G., Dauvergne, F., Gabriel, A., Hütsch, M., Marmotti, M., Sayers, Z., Stuhrmann, S., Thomas, J., Trame, C. & Stuhrmann, H. B. (1995). *Nucl. Instrum. Methods*, B**47**, 303–307.

Schütz, G., Knülle, M. & Ebert, H. (1994). *Resonant Anomalous X-ray Scattering*, edited by G. Materlik, C. J. Sparks & K. Fischer, pp. 535–556. Amsterdam: North Holland.

Sève, L., Tonnerre, J. M. & Raoux, D. (1998). *J. Appl. Cryst.* **31**, 700–707.

Sorensen, L. B., Cross, J. O., Newville, B., Ravel, B., Rehr, J. J., Stragier, H., Bouldin, C. E. & Woicik, J. C. (1994). *Resonant Anomalous X-ray Scattering, Theory and Applications*, edited by G. Materlik, C. J. Sparks & K. Fischer, pp. 389–420. Amsterdam: Elsevier Science.

Stuhrmann, S. (1997). Dissertation, Universität Hamburg, Germany.

Stuhrmann, S., Bartels, K. S., Hütsch, M., Marmotti, M., Sayers, Z., Thomas, J., Trame, C. & Stuhrmann, H. B. (1996). *Moscow Nauka Fizmatlit*, pp. 276–288 (In Russian.)

Stuhrmann, S., Braunwarth, R., Doose, R., Dauvergne, F., Gabriel, A., Knöchel, A., Marmotti, M., Thomas, J., Trame, C. & Lehmann, M. S. (1997). *J. Synchrotron Rad.* **4**, 298–310.

Stuhrmann, S., Braunwart, W. & Stuhrmann, H. B. (1995). *HASYLAB Annual Report 1995*, p. 1029. HASYLAB, DESY, Hamburg, Germany.

Stuhrmann, S., Hütsch, M., Trame, C., Thomas, J. & Stuhrmann, H. B. (1995). *J. Synchrotron Rad.* **2**, 83–86.

Thomas, J. (1997). Dissertation, Universität Hamburg, Germany.

Trame, C. (1997). Dissertation, Universität Hamburg, Germany.

Vettier, C. (1994). *Resonant Anomalous X-ray Scattering*, edited by G. Materlik, C. J. Sparks & K. Fischer, pp. 513–528. Amsterdam: North Holland.

Welsh, L. C., Symmons, M. F., Mitsch, C., Marseglia, E. A., Nave, C., Perham, R. N., Marvin, D. A., Stuhrmann, S., Trame, C. & Stuhrmann, H. B. (1995). *HASYLAB Annual Report 1995*, pp. 715–716. HASYLAB, DESY, Hamburg, Germany.